ECS Journal of Solid State
Science and Technology

OPEN ACCESS

Preferential Orientation and Surface Oxidation Control in Reactively Sputter Deposited Nanocrystalline SnO_2:Sb Films: Electrochemical and Optical Results

To cite this article: J. Montero *et al* 2014 *ECS J. Solid State Sci. Technol.* **3** N151

Preferential Orientation and Surface Oxidation Control in Reactively Sputter Deposited Nanocrystalline SnO_2:Sb Films: Electrochemical and Optical Results

J. Montero,[a,z] C. Guillén,[b] C. G. Granqvist,[a] J. Herrero,[b] and G. A. Niklasson[a]

[a]*Department of Engineering Sciences, The Ångström Laboratory, Uppsala University, SE-751 21 Uppsala, Sweden*
[b]*Department of Energy, Ciemat, E-28040 Madrid, Spain*

Antimony doped tin oxide is a versatile transparent electrical conductor. Many of its properties depend on the electronic band structure at the surface of a thin film–such as the position of the Fermi level, ionization potential I_p, optical gap energy, etc.–which in its turn is related to the surface termination given by the crystallographic orientation of the film. We prepared SnO_2:Sb films by reactive DC magnetron sputtering at different oxygen/argon ratios and found by X-ray diffraction that the crystallographic orientation could be changed from tetragonal (101) to tetragonal (110) as the oxygen content was raised. Electrochemical measurements showed that this change in preferential orientation was accompanied by an increase of I_p by more than 1 eV as a result of the modification of the oxidation state of tin atoms at the film's surface. Such alterations of I_p have a large impact on the electrochemical, photocatalytic and gas sensing behavior of the material. Moreover, preferential orientation control–and hence I_p tuning–allow the tailoring of SnO_2:Sb electrodes for various application by reducing the Schottky barrier.

Manuscript submitted July 23, 2014; revised manuscript received September 9, 2014. Published September 19, 2014.

Antimony doped tin oxide (SnO_2:Sb, denoted ATO) is a transparent conducting oxide[1–6] with a number of assets such as low cost, chemical inertness and non-toxicity. Thin films are readily made by sputter deposition as well as other techniques[2,6,7] and offer a multitude of applications in present and forthcoming technology. Thus ATO films are of interest for energy generation and savings[8–10] and can be used as electrodes for solar cells, light emitting diodes and electrochromic smart windows;[11–13] other applications include gas sensing[14] and photocatalysis.[15] Successful use of any material as an electrode, or as a gas sensor or photocatalyst, is to a large extent dependent on the position of its energy bands–i.e., locations of Fermi level, ionization potential I_p, optical gap energy, etc–in relation the vacuum level.[16–19]

In this work we deposited ATO thin films by reactive DC magnetron sputtering under different conditions and studied I_p by electrochemical measurements. In particular we found by X-ray diffraction (XRD) that the crystalline structure, and hence I_p, depended critically on the oxygen/argon ratio in the sputter plasma.

Experimental

ATO films were prepared by reactive DC magnetron sputtering onto unheated soda-lime glass substrates, 5×5 cm^2 in area and 3 mm thick. The target was a Sn:Sb disk (Sn:Sb = 95:5% by weight, 99.99% purity) with a diameter of 150 mm and 6 mm thickness. The deposition chamber was first evacuated to a base pressure of 2×10^{-7} mbar. The pressure was then raised to around 4×10^{-3} mbar by the inlet of oxygen and argon fluxes. denoted Φ_{O2} and Φ_{Ar}, respectively. The gas mixing ratio Γ, defined by

$$\Gamma = \Phi_{O2}/(\Phi_{O2} + \Phi_{Ar}), \quad [1]$$

ranged from 0.17 to 0.67. The discharge power density was set to 1.13 W/cm^2, and the deposition time was adjusted to reach a film thickness of ~400 nm as measured by a Dektak 3030 profilometer. Post-deposition annealing in air or N_2 was performed at temperatures of 250, 350 and 450°C by use of a quartz tube furnace in order to obtain films with different properties.

The crystalline structure of the samples was characterized by XRD using a Philips X'Pert-MPD diffractometer. The intensity ratio of the main characteristic XRD peaks for the tin dioxide cassiterite directions (101) and (110)–referred to as $I_{(101)}$ and $I_{(110)}$, respectively–was defined as

$$\psi = I_{(101)}/[I_{(101)} + I_{(110)}] \quad [2]$$

and used as parameter for structural characterization of the films. Optical transmittance and reflectance in the 300–2500 nm wavelength range were measured with a Perkin-Elmer Lambda 9 UV-VIS-NIR spectrophotometer. Electrochemical measurements were carried out in a two-electrode cell containing an electrolyte of 1 M lithium perchlorate in propylene carbonate. The ATO sample acted as working electrode and the reference electrode was a metallic Li foil. The open-circuit potential V_{oc} of the setup was recorded with the Li/Li$^+$ redox potential $E_{Li/Li+}$ as reference. Measurements were performed under Ar atmosphere in a glove box containing less than 0.6 ppm of H_2O.

Additional information regarding optical and electrical properties as a function of deposition parameters and post-deposition annealing processes, as well as X-ray photoelectron spectroscopy measurements performed on these ATO samples, can be found in our previous work.[2,7]

Theoretical Issues

Figure 1 shows the main equilibrium energy levels of an ATO film aligned according to the $E_{Li/Li+}$ level and the vacuum level E_{vac}. The energies of the different bands are designed as usual: E_{vbm} and E_{cbm} are the energy of the valence band maximum and the conduction band minimum, respectively. When an ATO sample is immersed in the electrolyte, the measured V_{oc} is given by the position of ATO's Fermi energy E_f in relation to the $E_{Li/Li+}$ level.[20] Therefore V_{oc}, together with the optical bandgap E_{g0}, will provide useful information about ATO's surface ionization potential and other band lineups. V_{oc} was multiplied by the electron charge q_e in order to get the energy barrier. E_{g0} was obtained from spectral optical data on the absorption coefficient, derived from transmittance and reflectance measurements and taking into account the direct nature of ATO's band-edge transition, as discussed elsewhere.[7,11]

As observed in Fig. 1, the work function W_f of ATO can be affected by variations in the position of E_f. These variations can ensue from an increasing free charge-carrier concentration, which is well-known as the Moss-Burstein shift[21,22] designed ΔE_{mb}. Moreover, as discussed by Körber et al.,[23] a modification the dipoles at the ATO surface will

[z]E-mail: jose.montero@angstrom.uu.se

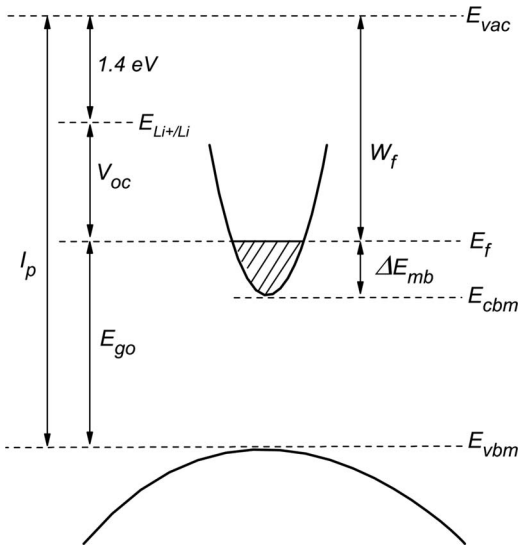

Figure 1. Equilibrium energy levels of an ATO film referred to the vacuum level E_{vac} and to the Li/Li$^+$ redox potential $E_{Li/Li+}$. The energy of the different bands and potential barriers are designed as usual (see text).

lead to a change of I_p. Therefore, we have selected I_p as the parameter of study in this work.

A determination of I_p comprises two steps: electrochemical measurement of V_{oc} and optical determination of E_{g0}. Since $E_{Li/Li+}$ is positioned 1.4 eV below E_{vac},[24–26] it is possible to obtain I_p as a function of V_{oc} and E_{g0} from

$$I_p = E_{g0} + q_e V_{oc} + \mathrm{E}_{\mathrm{Li/Li+}}, \qquad [3]$$

as also apparent from Fig. 1.

Results and Discussion

The preferential orientation of ATO films is strongly dependent on the oxygen content during the deposition processes, as evident from Fig. 2. The diffraction patterns shown in this figure correspond to a selection of representative samples deposited at various values of Γ and studied before and after different annealing treatments. Each diffractogram has a label indicating the characteristics of the film deposition process: the first number specifies Γ and the second the annealing temperature, and a letter N signifies treatment in nitrogen.

Figure 2 shows that ATO films deposited at low oxygen content, specifically $0.17 \leq \Gamma \leq 0.26$, have amorphous structure or polycrystalline cassiterite structure with (101) preferential orientation, depending on the annealing process. For $\Gamma > 0.26$, all samples exhibit polycrystalline structure with several clearly observable characteristic peaks corresponding to the cassiterite structure. The preferential orientation changes from (101) for samples deposited at $0.17 \leq \Gamma \leq 0.26$ to (110) for samples prepared at $\Gamma = 0.67$. Intermediate values, for example $\Gamma = 0.29$, result in a (211) preferential orientation, which corresponds to surface grain orientations between (101) and (110). Figure 3 shows the intensity ratio of the diffraction peaks, Ψ, as a function of Γ for three sets of samples, deposited at $\Gamma = 0.17$, 0.29 and 0.67, before and after the different annealing processes. As expected Ψ decreases as Γ is increased, i.e., with the increase of the oxygen flow, indicating a change in preferential orientation from (101) to (110) direction. Except for the amorphous samples deposited at $\Gamma = 0.17$, which crystallize after being annealed at 450°C in air or N_2, the annealing processes produce only small changes in Ψ and in the preferential orientation of the films.

A dependency of preferential orientation on oxygen content during deposition of tin oxide-based films has been reported previously in the literature, and the origin of this phenomenon has been the object of much discussion during the past years.[2,3,6,23,27–29] According to

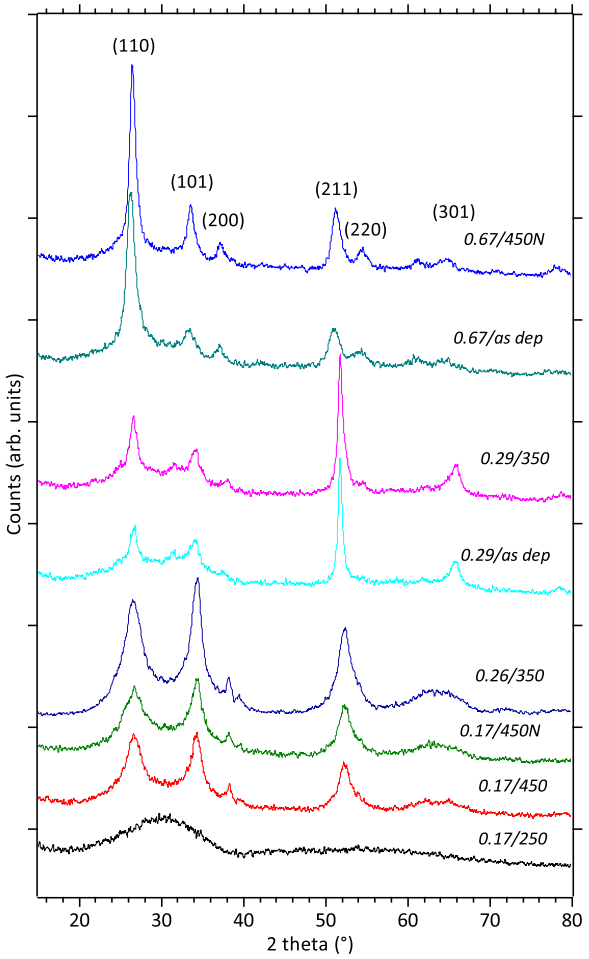

Figure 2. X-ray diffractograms of selected ATO samples with indicated reflection planes. Each curve has a label signifying the pertinent oxygen/argon gas flow Γ (first number) and the annealing temperature (second number). A letter N denotes annealing in nitrogen.

published data on calculated surface energies,[8,23,28] the reduced (101) surface, which is rich in Sn^{2+}atoms, is more stable at low oxygen chemical potentials, corresponding to samples deposited at low Γ values; the situation is reversed at high oxygen chemical potentials, and high Γ, where the oxidized (110) surface, which is rich in Sn^{4+} atoms is more stable. Therefore the change of the preferred film orientation in tin oxide can be related to differences in the (101) and (110) surface

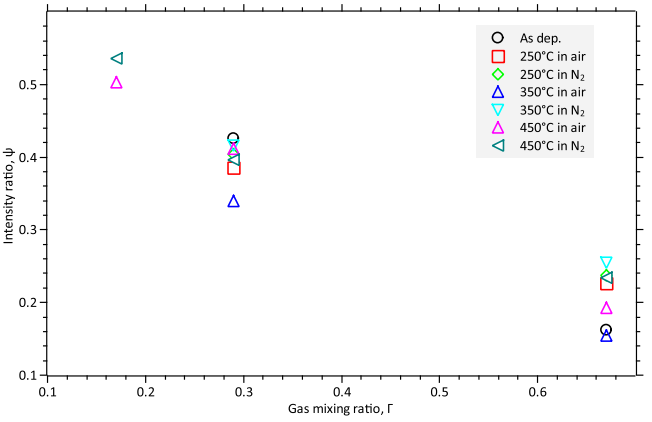

Figure 3. Intensity ratio of the diffraction peaks given by Ψ as a function of Γ for three sets of samples deposited at $\Gamma = 0.17$, 0.29 and 0.67, before and after different annealing processes.

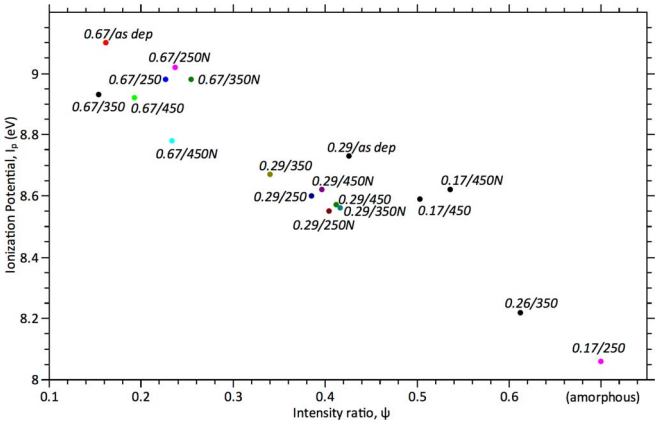

Figure 4. Ionization potential I_p vs. intensity ratio of the diffraction peaks given by Ψ for ATO films prepared under different conditions. The ionization potential for an amorphous sample is also shown (bottom right of the figure). Labels are designated as in Fig. 2.

stabilities and is also accompanied by a transition from Sn^{2+} to a Sn^{4+} surface termination (see work of Batzill and Diebold[8] and studies cited therein).

In order to study how a change in the oxidation state affects the band lineups at the film surface, I_p was measured for the different samples as explained in Sec. 3, and the obtained data plotted in Figure 4 as a function of Ψ, i.e., the intensity ratio of the XRD peaks corresponding to the (101) and (110) orientations. I_p for an amorphous sample has also been included in the graph. Samples deposited at $\Gamma = 0.67$ present (110) preferential orientation (i.e., low Ψ) and I_p values above 9 eV. As Ψ rises, I_p decreases gradually to around 8 eV in samples deposited at $0.17 \leq \Gamma \leq 0.26$ and exhibiting a (101) preferential orientation or amorphous structure. This variation in I_p by more than 1 eV supports the hypothesis that a change in the surface oxidation state–corresponding to an evolution from an oxidized (110) surface rich in Sn^{4+} atoms to a reduced (101) surface rich in Sn^{2+} atoms–can modify I_p by more than 1 eV as a result of surface dipole modifications.[30] The results plotted in Fig. 4, obtained by electrochemical measurements, are in agreement with data published by Körber et al. who measured I_p by ultraviolet photoelectron spectroscopy.[23,28,30]

The electrochemical measurements provide information on the oxidation state of the tin atoms at the film surface. This information can be complemented by a study of the film's refractive index *n*. Semi-empirical models have pointed out that a high proportion of Sn^{2+} atoms, not only in the surface but also inside the tin oxide thin film, causes a decrease of *n*.[31] Figure 5 shows *n* at a wavelength of

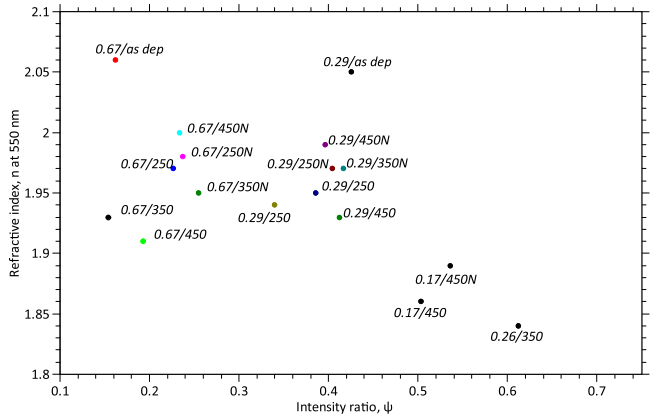

Figure 5. Refractive index *n* at 550 nm vs. crystalline orientation given by Ψ for ATO films prepared under different conditions. Labels are designated as in Fig. 2.

550 nm, as calculated from the sample transmittance by the well-established Swanepoel method,[32] vs. Ψ. Samples deposited at low Γ and exhibiting a (101) preferential orientation show the lowest values, i.e., highest concentration of Sn^{2+}. However the dependency of *n* on Ψ is not as clear as the one observed for I_p, on Ψ, and in the former case the characteristics of the annealing processes play an important role. This dependency is expected because parameters such as film density and porosity affect *n* in addition to the oxidation state of the tin atoms.

Conclusions

Sputter deposited SnO_2:Sb thin films display a change in their preferential orientation from the tetragonal (101) to the (110) direction as the oxygen concentration during the deposition process is increased. This modification in preferential orientation is accompanied by a change in the oxidation of the surface from a reduced (101) to an oxidized (110) state, which in its turn is followed by an increase of the ionization potential by more than 1 eV as measured electrochemically. Such changes of I_p have a large impact on the electrochemical, photocatalytic and gas sensing behavior of the material. Furthermore preferential orientation control, and hence I_p tuning, will allow tailoring of SnO_2:Sb electrodes for various application by reducing the Schottky barrier.

Acknowledgments

This work has been supported by the Swedish Research Council and by the European Research Council under the European Community's Seventh Framework Program (FP7/2007-2013)/ERC Grant Agreement No. 267234 (GRINDOOR).

References

1. C. Kilic and A. Zunger, *Phys. Rev. Lett.*, **88**, 095501 (2002).
2. J. Montero, C. Guillén, and J. Herrero, *Sol. Energy Mater. Sol. Cells*, **95**, 2113 (2011).
3. J. Boltz, D. Koehl, and M. Wuttig, *Surf. Coat. Technol.*, **205**, 2455 (2010).
4. J. Kong, H. Deng, P. Yang, and J. Chu, *Mater. Chem. Phys.*, **114**, 854 (2009).
5. D. G. Stroppa, L. A. Montoro, A. Beltran, T. G. Conti, R. O. da Silva, J. Andres, E. Longo, E. R. Leite, and A. J. Ramirez, *J. Am. Chem. Soc.*, **131**, 14544 (2009).
6. B. Stjerna, E. Olsson, and C. G. Granqvist, *J. Appl. Phys.*, **76**, 3797 (1994).
7. J. Montero, J. Herrero, and C. Guillén, *Sol. Energy Mater. Sol. Cells*, **94**, 612 (2010).
8. M. Batzill and U. Diebold, *Prog. Surf. Sci.*, **79**, 47 (2005).
9. C. G. Granqvist, *Sol. Energy Mater. Sol. Cells*, **91**, 1529 (2007).
10. E. Fortunato, D. Ginley, H. Hosono, and D. C. Paine, *MRS Bull.*, **32**, 242 (2007).
11. D. S. Ginley, H. Honoso, and D. C. Paine, editors, *Handbook of Transparent Conductors* (Springer, New York, 2010).
12. S. Green, J. Backholm, P. Georén, C. G. Granqvist, and G. A. Niklasson, *Sol. Energy Mater. Sol. Cells*, **93**, 2050 (2009).
13. B. G. Lewis and D. C. Paine, *MRS Bull.*, **25**, 22 (2000).
14. G. Eranna, B. C. Joshi, D. P. Runthala, and R. P. Gupta, *Crit. Rev. Solid State Mater. Sci.*, **29**, 111 (2004).
15. J. C. M. Brokken-Zijp, O. L. J. van Asselen, W. E. Kleinjan, R. van de Belt, and G. de With, *J. Nanotechnol.*, **2011**, 106254 (2011).
16. A. Klein, C. Körber, A. Wachau, F. Säuberlich, Y. Gassenbauer, S. P. Harvey, D. E. Proffit, and T. O. Mason, *Materials*, **3**, 4892 (2010).
17. N. Bârsan and U. Weimar, *J. Electroceram.*, **7**, 143 (2001).
18. N. Bârsan and U. Weimar, *J. Phys.: Cond. Matter*, **15**, R813 (2003).
19. M. Gratzel, *Nature*, **414**, 338 (2001).
20. K. Rajeshwar, *Fundamentals of Semiconductor Electrochemistry and Photoelectrochemistry* (Wiley-VCH, Weinheim, Germany, 2007).
21. T. S. Moss, *Proc. Phys. Soc. London*, **67**, 775 (1954).
22. E. Burstein, *Phys. Rev.*, **93**, 632 (1954).
23. C. Korber, P. Agoston, and A. Klein, *Sens. Actuators B*, **139**, 665 (2009).
24. R. Memming, *Semiconductor Electrochemistry* (Wiley-VCH, Weinheim, Germany, 2008).
25. D. R. Lide, *CRC Handbook of Chemistry and Physics, 79th Edition* (CRC Press, Boca Raton, FL, 1998).
26. D. E. Scaife, *Solar Energy*, **25**, 41 (1980).
27. B. Stjerna and C. G. Granqvist, *Appl. Phys. Lett.*, **57**, 1989 (1990).
28. C. Korber, J. Suffner, and A. Klein, *J. Phys. D: Appl. Phys.*, **43**, 055301 (2010).
29. K. Suzuki and M. Mizuhashi, *Thin Solid Films*, **97**, 119 (1982).
30. A. Klein, C. Körber, A. Wachau, F. Säuberlich, Y. Gassenbauer, R. Schafranek, S. P. Harvey, and T. O. Mason, *Thin Solid Films*, **518**, 1197 (2009).
31. S. Goldsmith, E. Çetinörgü, and R. L. Boxman, *Thin Solid Films*, **517**, 5146 (2009).
32. R. Swanepoel, *J. Phys. E: Sci. Instrum.*, **16**, 1214 (1983).